Electrochimica Acta 476 (2024) 143717

Contents lists available at ScienceDirect

Electrochimica Acta

journal homepage: www.journals.elsevier.com/electrochimica-acta

Effect of nanoclays on the electrochemical performance of LbL catechol sensors

C. Garcia-Hernandez [a,b,*], C. Garcia-Cabezon [a,b], M.L. Rodriguez-Mendez [b,c], F. Martin-Pedrosa [a,b]

[a] Materials Engineering, E.I.I., Universidad de Valladolid, Valladolid 47011, Spain
[b] BioecoUVA Research Institute, Universidad de Valladolid, Valladolid 47011, Spain
[c] Group UVASENS, E.I.I., Universidad de Valladolid, Valladolid 47011, Spain

ARTICLE INFO

Keywords:
Halloysite nanotubes
Copper phthalocyanine
Polyethylenimine
Tyrosinase
LbL sensors

ABSTRACT

Halloysite nanotubes (HNTs) are excellent candidates to improve the immobilization of electroactive materials or enzymes due to their tubular structure and properties. In this work, an improved LbL based catechol sensor has been developed using a combination of sensing materials with complementary activity. These include sulfonated copper phthalocyanine ($CuPc^{SO3-}$) acting as electrocatalytic material, poly(ethyleneimine) (PEI) to increase the charge injection efficiency and the increase of the surface provided by HNTs. The LbL film has been used as the sensing platform to deposit tyrosinase in order to further enhance the performance of the developed sensor towards catechol. The LbL films were characterized by using UV–Vis, FTIR and cyclic voltammetry. The limits of detection, repeatability and reproducibility of the sensors and the biosensor were evaluated. The limits of detection were 1.23 $\mu mol \cdot L^{-1}$ for the optimized (PEI/$CuPc^{SO3-}$) sensor, 0.987 $\mu mol \cdot L^{-1}$ for the (PEI/HNT/PEI/$CuPc^{SO3-}$) sensor and 0.938 $\mu mol \cdot L^{-1}$ for the (PEI/HNT/PEI/$CuPc^{SO3-}$)-Tyrosinase sensor.

1. Introduction

In the last decades, important advances have been made in the field of electrochemical sensors thanks to the introduction of new platforms for sensors design, such as nanotechnological materials (i.e. conducting polymers, metallophtacocyanines, metal nanoparticles, etc.) and nano-structured architectures (carbon nanotubes, LbL films, self-assembly monolayers, etc.) which have improved their sensitivity. The choice of materials for the sensing units is crucial to obtain a high performance. Metallophthalocyanines (MPcs) (N4-macrocyclic metal complexes) are molecular organic semiconductors that have been widely used in the construction of electrochemical sensors since they exhibit remarkable electrochemical and electrocatalytic properties owing to their ability to accept and donate electrons, either from central metal ions or 18-π-conjugated ring systems [1–4]. Moreover, organic semiconductors are also very attractive as building blocks in organic-based devices where the injection of charge into the organic semiconductor is sourced from a conductive electrode [5]. Electron injection into the organic semiconductor can be achieved using an electrode that matches the highest occupied molecular orbital (HOMO) of the organic semiconductor. In this sense, the charge injection efficiency increases as the barrier height at the interface decreases [5–8]. For this purpose, several strategies have been carried out to minimize the energy barrier at the metal/organic semiconductor interface to improve the charge injection efficiency [5]. One of them is the use of insulating polymers containing simple aliphatic amine groups, such as the branched polyethylenimine (PEI), that have demonstrated to be a surface modifier that allows the fabrication of electrodes for efficient electron injection, reducing the energy barrier for electron injection through the intrinsic molecular dipole moments associated with the neutral amine groups [9]. Thus, the use of PEI in electrochemical sensors lead to a better energy level alignment between the metal electrode and the organic semiconductor.

On the other hand, in the fabrication of electrochemical sensors based on nanomaterials it is important to get carriers for nanomaterials that help to improve their dispersion and/or increase the electroactive area and, for this purpose, nanoclays are good candidates due to their high surface area. This material is defined as natural or synthetic clay minerals with a layered structure and with at least one dimension in the nano-scale range [10,11]. Halloysite is a two-layered aluminosilicate clay mineral with the empirical formula $Al_2Si_2O_5(OH)_4 \cdot 2H_2O$.

* Corresponding author at: Department of Materials Science, Universidad de Valladolid, Paseo del Cauce, 59, 47011 Valladolid, Spain.
E-mail address: celia.garcia.hernandez@uva.es (C. Garcia-Hernandez).

https://doi.org/10.1016/j.electacta.2023.143717
Received 23 May 2023; Received in revised form 5 December 2023; Accepted 24 December 2023
Available online 25 December 2023

Halloysite nanotubes (HNTs) are hollow tubes with diameters (inner and outer) smaller than 100 nanometers and lengths ranging from 0.2 to 1.5 μm [10]. A monolayer HNT $Al_2Si_2O_5(OH)_4{\cdot}nH_2O$ refers to the so-called halloysite (10 Å, $n = 2$). Dehydrating the HNT by heating leads to halloysite (7 Å, $n = 0$). The charge (zeta potential) behavior of the HNT particles is described as mostly negative surface potential of SiO_2 (at pH 6–7) and a small contribution from the positive Al_2O_3 inner surface (at pH 2–8) [11].

HNTs exhibit interesting properties such as their swelling, adsorbent and cation exchange capacity, plasticity, high surface area, natural occurrence and cytocompatibility [12,13]. Due to their hollow tubular shape and cation exchange capacity, HNTs have been used in the fabrication of sensors by incorporating electroactive ions or enzymes, among other, to be applied in the medical, environmental and food industry [10,12–15]. Moreover, in comparison to carbon nanotubes, HNTs have some important advantages like their low-cost, non-toxicity, availability and their environmentally safe and ease to process [14,16,17]. Furthermore, the inner and outer sides of HNTs present a particular surface chemistry which is one of the major advantages of this material in order to achieve a selective functionalization of the lumen of HNTs and the outer surface [13]. In the field of electrochemical sensors, HNTs have been used due to their attractive aforementioned properties in several analyte identification such as hydrogen peroxide [18–22], nitrites [23,24], glucose [22,25,26], ascorbic acid [27], dopamine [28], hydrazine [29] and mercury in aqueous media [30]. HNTs have also been implemented in the field of enzymatic electrochemical biosensors to improve their specificity, selectivity and sensitivity. In this sense, sensors must also provide properties such as good limit of detection, response time, stability and/or linearity. However, only few works of HNTs-based biosensors have been reported based on glucose oxidase [31], lactase [32] and peroxidase [33]. For enzyme-based sensors, the specificity must be maintained even when altering temperature and pH and, moreover, regenerated again during the reaction. In addition, direct electron transfer between the enzyme and the electrode surface must be achieved. For this purpose, HNTs can be used to improve enzyme immobilization and thus enhance the performance of the sensors due to their high surface area and also their high loading capacity as they have an empty lumen that can be a suitable substrate for the loading of different molecules. Furthermore, other properties such as the cost, biocompatibility, hollow tube structure and light density raise even more this material like an advanced nanomaterial for biosensor applications. Regarding the hollow tube structure, it is interesting to note that Kummar Krishnan et al. have reported the advantage of the curve surface of HNTs which helps to decrease the attraction between two nearby enzymes and access the multilinking point and, therefore, reduces the enzyme aggregation on the surface ensuring their biocatalytic activity [31].

In this work, we report a novel electrochemical nanostructured sensor using HNTs in order to improve the electrocatalytic performance of a copper phatholcyanine based sensor. For this purpose, sensors were fabricated by the LbL technique due to their low-cost and versatility to prepare nanostructured films in addition to the simplicity of the required equipment and the particular advantage of the use of mild conditions (e.g. aqueous solutions). The electrochemical responses of the sensors were tested towards the polyphenol catechol, which is a phenolic group of interest in the oxidation process of many foods. Moreover, to go a step further, it has been evaluated the use of a tyrosinase-based biosensor in order to corroborate the high capacity of the HNTs to immobilize enzymes.

2. Experimental

2.1. Chemicals

All chemicals and solvents were of reagent grade and used without further purification. Copper(II) phthalocyanine tetrasulfonic acid tetrasodium salt ($CuPc^{SO3-}$); poly(ethyleneimine) (PEI, branched, 25 kDa); halloysite nanoclays (HNT) (30–70 nm × 1–3 μm), and the phenol oxidase enzyme tyrosinase (from mushroom, activity ≥1000 $U{\cdot}mg^{-1}$) (Tyr) were purchased from Sigma-Aldrich (St. Louis, MO, USA). The halloysite nanoclay was dehydrated by heating at 210 °C for 3 h prior to use it. Phosphate buffer (0.01 M; pH 7.0) was used to prepare all the solutions. 10^{-3} $mol{\cdot}L^{-1}$ stock solutions of catechol were prepared by solving the corresponding compound in KCl solution (0.1 $mol{\cdot}L^{-1}$).

2.2. Apparatus

Layer by layer films were deposited onto ITO glass substrate using a ND-R 11/2 Rotary Coater (Nadetech Innovations, Navarra, Spain). Voltammetric measurements were obtained using a potentiostat/galvanostat PARSTAT 2273 (Princeton Applied Research, Oak Ridge, TN, USA) and an electrochemical cell of three-electrode. The LbL sensors were used as the working electrode; the reference electrode was Ag|AgCl/KCl 3 $mol{\cdot}L^{-1}$ and the counter electrode was a platinum sheet with a surface area of 1 cm^2. Fourier transform infrared (FTIR) spectra of the films deposited on ZnSe were obtained from 4000 to 400 cm^{-1} using a Jasco Model FT/IR-6600 Spectrometer (Tokyo, Japan). The software used for FTIR data collection was Spectra Manager II (Jasco, Tokyo, Japan). Before the analysis the instrument was purged with nitrogen for 10 min. As reference, the background spectrum of air (100 BKG) was collected before the acquisition of the sample spectrum. The spectra were recorded at 26 °C with a resolution of 2 cm^{-1} and 300 scans were averaged for each spectrum. UV–Vis spectra were registered from 300 to 800 nm in a Shimadzu UV-1603 spectrophotometer (Kyoto, Japan).

2.3. LbL sensors preparation

ITO glass substrates (1 cm^2 surface area) were used as the substrate. Prior to the film deposition, the substrates were washed in an ultrasonic bath with acetone and gently rinsed with deionized water (MilliQ).

2.3.1. Preparation of $(PEI/CuPc^{SO3-})_n$ LbL sensors

The LbL films were grown using PEI as the positive layer and $CuPc^{SO3-}$ as the negative layer. PEI solution of 1 $g{\cdot}L^{-1}$ and phthalocyanine solution of $5{\cdot}10^{-4}$ $mol{\cdot}L^{-1}$ both in phosphate buffer (0.01 $mol{\cdot}L^{-1}$, pH 7.0) were used to build the films. LbL films were fabricated by successive immersions of the ITO substrate in the PEI and the phthalocyanine solution. Fig. 1 illustrates the sequence of the immersions: (1) PEI solution (3 min); (2) deionized water to remove excess of non-adsorbed PEI (30 s); (3) $CuPc^{SO3-}$ solution (5 min); (4) deionized water to remove the excess and non-adsorbed $CuPc^{SO3-}$ (30 s). After these four steps a complete sequence is deposited onto the ITO substrate ($n = 1$). This procedure was also followed for $n = 5$ (that is, 5 sequences) and for $n = 10$ (10 sequences).

2.3.2. Preparation of $(PEI/HNT/PEI/CuPc^{SO3-})_n$ LbL sensors

The LbL films prepared with HNT were grown using PEI as the positive layer, and HNT and $CuPc^{SO3-}$as the negative layers. PEI and $CuPc^{SO3-}$ solutions were the same as described before. The HNT solution used was 1 $mg{\cdot}L^{-1}$ in deionized water. The sequence of the film deposition is shown in Fig. 2: (1) PEI solution (3 min); (2) deionized water to remove excess of non-adsorbed PEI (30 s); (3) HNT solution (10 min); (4) deionized water to remove excess of non-adsorbed HNT (30 s); (5) PEI solution (3 min); (6) deionized water to remove excess of non-adsorbed PEI (30 s); (7) $CuPc^{SO3-}$ solution (5 min); (8) deionized water to remove the excess and non-adsorbed $CuPc^{SO3-}$ (30 s). After these eight steps a complete sequence is deposited onto the ITO substrate ($n = 1$). In this case, the procedure was also followed for $n = 5$ and for $n = 10$.

2.3.3. Preparation of $(PEI/HNT/PEI/CuPc^{SO3-})_n$ -Tyr-LbL sensors

$(PEI/HNT/PEI/CuPc^{SO3-})_n$-Tyr-biosensors were prepared by

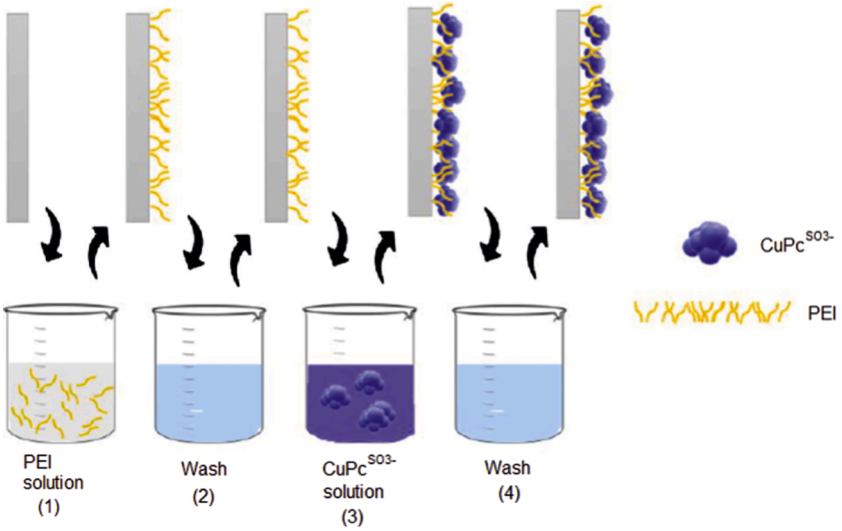

Fig. 1. Preparation of $(PEI/CuPc^{SO3-})_n$ LbL films.

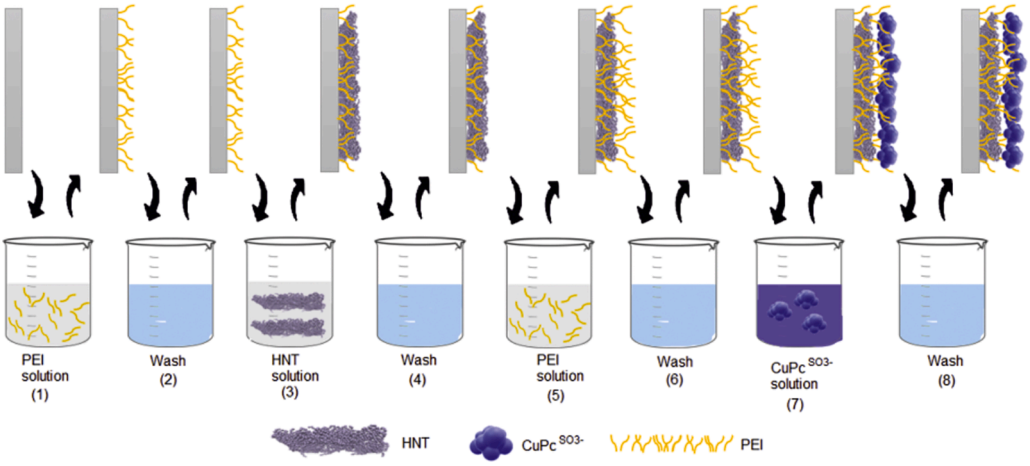

Fig. 2. Preparation of $(PEI/HNT/PEI/CuPc^{SO3-})_n$ LbL films.

depositing tyrosinase onto the $(PEI/HNT/PEI/CuPc^{SO3-})_n$ sensors. For this purpose, a solution of 5 mg·mL^{-1} of tyrosinase in 0.01 mol·L^{-1} phosphate buffer (pH 7.0) was used. Firstly, the LbL sensor was immersed in 0.01 mol·L^{-1} phosphate buffer (pH 7.0) for 2 min, following by 5 min of immersion in glutaraldehyde (2.5 % v/v, buffer solution) and dried in air at room temperature for 15 min. Then, 50 µL of tyrosinase solution was deposited onto the LbL sensor by drop-casting, dried at room temperature for approximately 45 min and, finally, the LbL biosensor was rinsed with phosphate buffer to remove any unbound enzyme and stored at 4 °C.

2.4. Electrochemical measurements

Cyclic voltammetry was carried out from −1.0 V to +1.2 V (vs. Ag/AgCl) with a scan rate of 0.1 V·s^{-1}, except when indicated otherwise. A KCl solution (0.1 mol·L^{-1}) was employed as the electrolytic medium in electroanalysis experiments. The influence of the potential sweep rate was studied in 10^{-3} mol·L^{-1} catechol in 0.1 mol·L^{-1} KCl, while varying the scan rates from 0.01 to 2.0 V·s^{-1}. The limits of detection (LD) were calculated from peak current responses taken from voltammograms recorded at different concentrations from 10 to 138 µmol·L^{-1}, following the "3·SD/m" criterion, where "m" is the slope of the calibration graph and "SD" was estimated as the standard deviation (n = 5) of the voltammetric signals at the concentration level corresponding to the lowest concentration of the calibration plot.

The repeatability of the voltammograms was evaluated from 10 repetitions on each sample. The reproducibility of data provided by the LbL films was evaluated by comparing data provided by 3 sensors measuring identical samples in different days.

3. Results and discussion

3.1. UV–Vis characterization

The LbL films were prepared using the procedure described above. The growth of the films was monitored after each sequence by UV–Vis absorption spectroscopy. Fig. 3 shows the UV–Vis spectra of the LbL components separately. As can be observed, only the $CuPc^{SO3-}$ exhibited absorbance at shorter wavelengths (Soret band at 336 nm) from the π-π* transition in the macrocyclic ring of phthalocyanine and at longer wavelengths, the Q band at 608 nm (dimeric) and a shoulder at 663 nm (monomeric) which are attributed to the HOMO→LUMO electronic transitions of the π electrons between the central metal and axial ligands in the phthalocyanine structure [34–36]. As expected, the PEI and HNT do not show any absorbance in the studied range.

Fig. 4 shows the UV–Vis spectra of $(PEI/CuPc^{SO3-})_n$ and $(PEI/HNT/PEI/CuPc^{SO3-})_n$ LbL films and the linear correlation between the absorbance and the number of layers for both systems. The absorbance

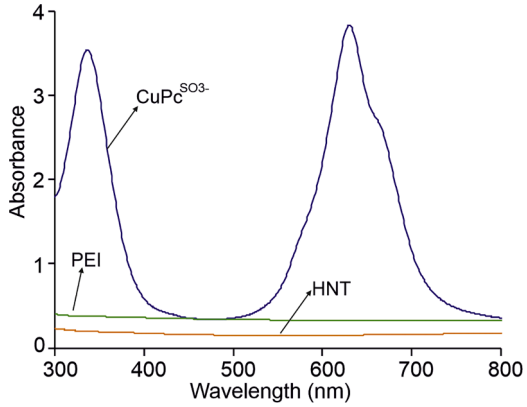

Fig. 3. UV–Vis spectra of $CuPc^{SO3-}$, HNT and PEI water solutions.

of the Q band increased linearly after the deposition of each sequence confirming the good quality of the deposition and the uniform growth of the LbL films. The linearity regression coefficient for $(PEI/HNT/PEI/CuPc^{SO3-})_n$ LbL films was higher than for $(PEI/CuPc^{SO3-})_n$ representing a better and more uniform deposition of the sequences, that can also be observed in the UV–Vis spectra where a similar amount of material is transferred onto the substrate per sequence confirming a more uniform growth of the LbL films. Moreover, for both LbL sensors, the quality of the films, and hence the linearity regression coefficient, decreased for more than 10 sequences. In fact, in some depositions carried out for $(PEI/CuPc^{SO3-})_n$, it was observed that after a sequence the absorbance decreased below that the obtained in the previously sequence as illustrated in Fig. 4 after the sequence number 5 and after the number 9. This result can mean that there was a loss of material during the procedure.

On the other hand, the amount of $CuPc^{SO3-}$ transferred onto the substrate after each sequence was higher for $(PEI/HNT/PEI/CuPc^{SO3-})_n$ than for $(PEI/CuPc^{SO3-})_n$ LbL films (Fig. 4c) which clearly confirms the influence of the HNT in facilitating the adsorption of $CuPc^{SO3-}$ in the LbL system. The preparation method was highly reproducible and coefficients of variation calculated from the maximum absorbance after 10 sequences were lower than 3 %.

3.2. FTIR characterization

The FTIR spectra of the LbL films and of all three compounds forming the films were collected using zinc selenide (ZnSe) as the substrate. Fig. 5a-c shows the spectra of bare materials. The FTIR spectrum corresponding to PEI contains two characteristic bands at 1541 cm^{-1} and at 1422 cm^{-1} corresponding to the bending of imine N—H bond and to the C—H bond, respectively, the N—H stretching at 3500 cm^{-1}, the C—H stretching at 2870 cm^{-1} and 2798 cm^{-1} and the C—N stretching at 1040 cm^{-1}[37,38].

The main peaks for $CuPc^{SO3-}$ appeared at a wavenumber of 3500 cm^{-1} associated with O—H stretching in the SO_3–H group, the vibration stretching of the bonds C—N and C—C can be seen at 1600 cm^{-1} and 1480 cm^{-1}, respectively. The peaks corresponding to the stretching of O—S—O appeared at 978–1127 cm^{-1} and 1263–1453 cm^{-1}, the peak obtained at 875 cm^{-1} is due to the presence of Cu-ligand and the vibrational stretching seen at 692–770 cm^{-1} indicates the presence of a phthalocyanine ring [37,39,40].

The FTIR spectrum of the HNT clay displayed a peak from the O—H deformation of the inner hydroxyl groups at 857 cm^{-1}, the peak corresponding to the stretching of the Si—O—Si bond at a wavenumber of 981 cm^{-1} and the reflection one at 1068 cm^{-1}. Finally, the stretching vibration due to the external and internal O—H groups of HNTs were observed at the wavenumbers of 3565 cm^{-1} and 3638 cm^{-1} [19,32,41].

The FTIR spectra of the $(PEI/CuPc^{SO3-})_{10}$ and $(PEI/HNT/PEI/CuPc^{SO3-})_{10}$ sensors were studied in order to identify the interaction

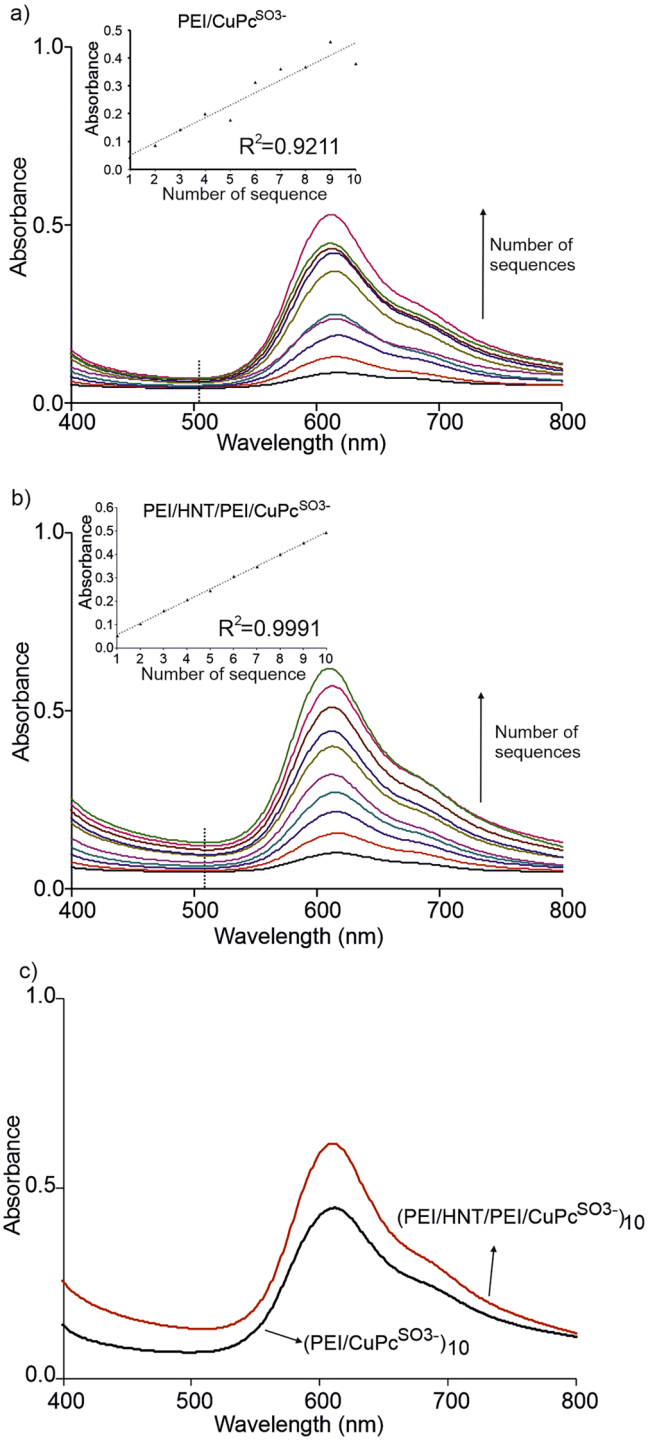

Fig. 4. UV–Vis characterization of (a) $(PEI/CuPc^{SO3-})_n$ and (b) $(PEI/HNT/PEI/CuPc^{SO3-})_n$ LbL films (from $n = 1$ to $n = 10$) with the corresponding linear correlation between absorbance near 608 nm vs. number of sequences. c) Comparison between the UV–Vis spectra of $(PEI/CuPc^{SO3-})_{10}$ LbL films and $(PEI/HNT/PEI/CuPc^{SO3-})_{10}$.

between each material in the composition of the LbL films and, therefore, corroborate their correct adhesion by electrostatic forces. In Fig. 5d, the PEI bands at 1580 cm^{-1} and 1430 cm^{-1} assigned to N—H and C—H bending were also found in the $(PEI/CuPc^{SO3-})$ LbL films with small changes in position. The appearance of a band at a wavenumber of 3500 cm^{-1} due to the N—H stretching group from the PEI and the C—H stretching at 2870 cm^{-1} and 2802 cm^{-1} and the C—N stretching at 1340

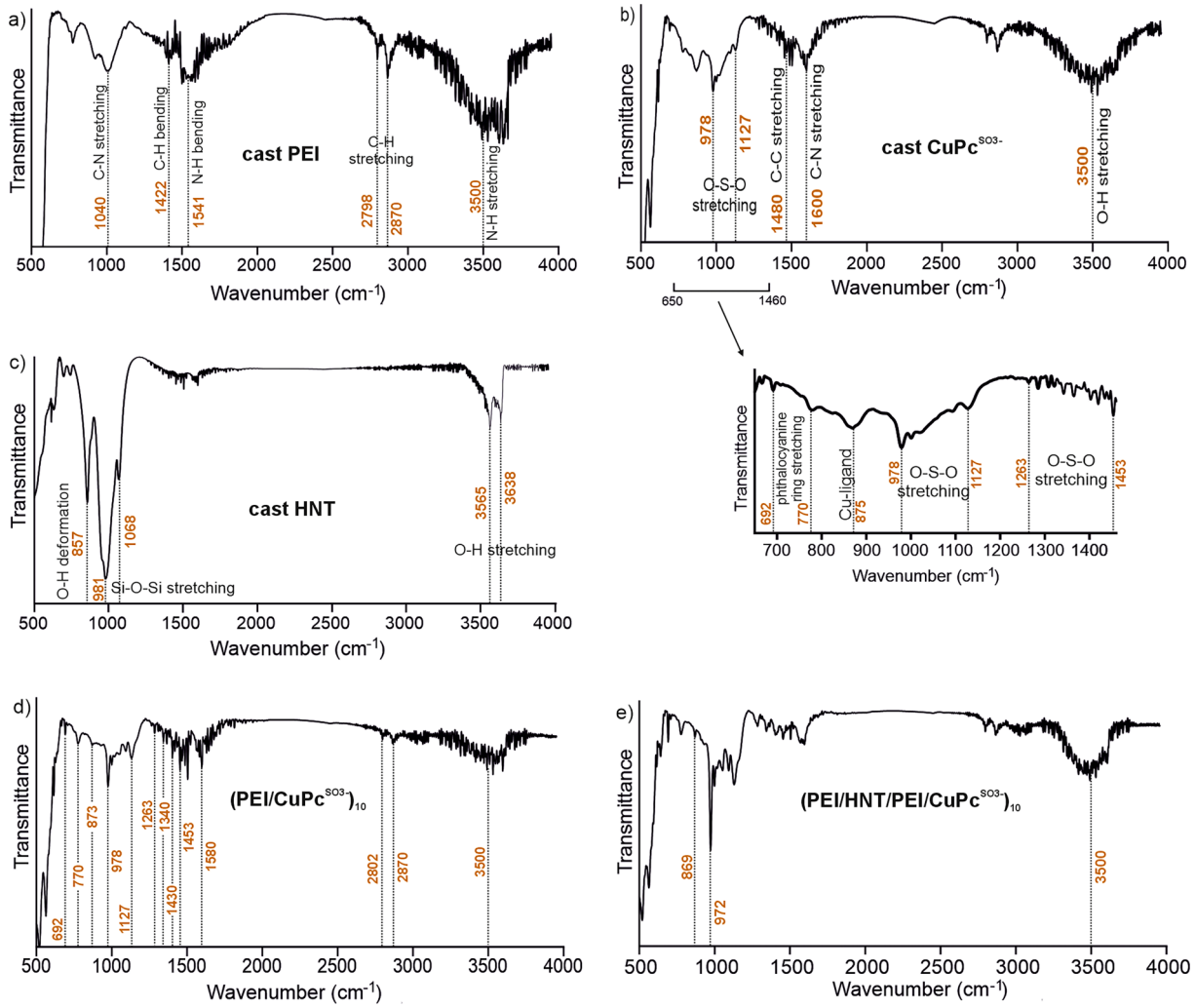

Fig. 5. a-c) Comparison between the FTIR spectra of each LbL component (cast), d) FTIR spectrum of $(PEI/CuPc^{SO3-})_{10}$ and e) FTIR spectrum of $(PEI/HNT/PEI/CuPc^{SO3-})_{10}$ LbL films.

cm^{-1} were also identified. Additionally, the bands corresponding to $CuPc^{SO3-}$ at 978–1127 cm^{-1} and 1263–1453 cm^{-1} due to the stretching of O—S—O can be seen, as well as the peak obtained at 873 cm^{-1} due to the Cu–ligand and the vibrational stretching at 692–770 cm^{-1} of the phthalocyanine ring. These results suggest the formation of LbL films between PEI and $CuPc^{SO3-}$ in a supramolecular level interaction by the formation of salt bridges of SO_3—NH_3, which includes hydrogen bonding and electrostatic interaction, between H atom from protonated amine group from PEI and O atom of sulfonic group from $CuPc^{SO3-}$ [37,42].

On the other hand, in Fig. 5e, when HNT is incorporated into the LbL structure, the $(PEI/HNT/PEI/CuPc^{SO3-})$ films showed some signals due to HNT, such as the peak from the O—H deformation of the inner hydroxyl groups shifted at 869 cm^{-1}. The peak corresponding to the stretching of the Si—O—Si bond and the peak of the stretching of O—S—O from the sulfonic group of the $CuPc^{SO3-}$ appeared overlapped and shifted at 972 cm^{-1}, indicating that these polar groups can be involved in an electrostatic interaction [37]. Moreover, the stretching vibration due to the external and internal O—H groups of HNTs at 3565 cm^{-1} and 3638 cm^{-1} were not observed in the FTIR spectrum of $(PEI/HNT/PEI/CuPc^{SO3-})$ films due to when the external hydroxyl groups of HNTs form the interactions with the amine groups of PEI these bands could shift blue and, thus, they were overlapped with the band at 3500 cm^{-1} corresponding to the stretching of the N—H bond from the PEI [41].

3.3. Electrochemical characterization

The electrochemical responses of the LbL sensors were analysed in catechol using cyclic voltammetry. A solution of KCl 0.1 $mol{\cdot}L^{-1}$ was used as the supporting electrolyte and the responses of the sensors were

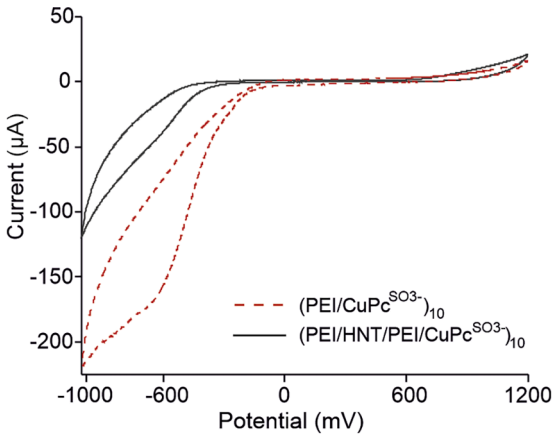

Fig. 6. Voltammetric responses of the $(PEI/CuPc^{SO3-})_{10}$ and $(PEI/HNT/PEI/CuPc^{SO3-})_{10}$ LbL sensors in KCl (0.1 $mol{\cdot}L^{-1}$).

first cycled (10 cycles) in the solution to adjust the films to the environment. Fig. 6 shows the responses of (PEI/$CuPc^{SO3-}$)$_{10}$ and (PEI/HNT/PEI/$CuPc^{SO3-}$)$_{10}$ sensors in KCl where it is observed that the films do not have peaks of interest.

The voltammograms of (PEI/$CuPc^{SO3-}$)$_n$ and (PEI/HNT/PEI/$CuPc^{SO3-}$)$_n$ immersed in catechol 10^{-3} mol·L^{-1} in KCl are shown in Fig. 7 for different number of sequences (n = 1, 5 and 10) in order to determine the effect of "n" in the electrochemical responses. Results of both LbL structures clearly exhibits that the higher number of sequences, the greater values of intensities for the anodic and cathodic responses. During the oxidation, catechol was oxidized to form 1,2-benzoquinone exhibiting 2 anodic peaks, respectively, while during the reverse scan, quinones were reduced to the phenolic compound displaying a broad peak. In addition, the (PEI/HNT/PEI/$CuPc^{SO3-}$) sensors showed higher intensities towards catechol than the (PEI/$CuPc^{SO3-}$) sensors, as well as exhibited peaks with a shape better defined and a more stable anodic potential, especially in the second peak of the oxidation. The values of potentials and intensities of the peaks are summarized in Table 1. This result corroborates that the implementation of HNT in the LbL films leads to a better adhesion of the phthalocyanine and, therefore, to a significant enhancement in its electrocatalytic behavior.

The (PEI/HNT/PEI/$CuPc^{SO3-}$)$_{10}$ LbL films were also used as the electron mediator in a tyrosinase-based biosensor, (PEI/HNT/PEI/$CuPc^{SO3-}$)$_{10}$-Tyr, as tyrosinase is selective to the oxidation of o-diphenols such as catechol. For this purpose, the LbL sensor used was that with HNT and with a number of LbL sequences of 10 considering that this sensor performed the better voltammetric behaviour in catechol as stated before. The as-prepared biosensors immersed in catechol do not exhibit a drastic increase in the intensity of the peaks as it has been reported in other works. However, a clear and notable improvement in the reversibility of the peaks was observed, and besides only one oxidation peak was observed instead of two peaks, occurring the oxidation/reduction of the catechol at lower potentials than for the non-enzymatic sensors (Fig. 8). This result demonstrates that the LbL films containing HNT facilitate the electron transfer and the synergistic effect between the components is clear.

Table 1
Potentials and intensities obtained in catechol 10^{-3} mol·L^{-1} in KCl (0.1 mol·L^{-1}).

LbL sensor	Anodic peaks		Cathodic peaks	
	Pontential (mV)	Intensity (μA)	Pontential (mV)	Intensity (μA)
(PEI/$CuPc^{SO3-}$)$_1$	420 1050	65 220	125	−75
(PEI/$CuPc^{SO3-}$)$_5$	425 950	85 300	140	−110
(PEI/$CuPc^{SO3-}$)$_{10}$	500 975	110 340	125	−130
(PEI/HNT/PEI/$CuPc^{SO3-}$)$_1$	390 1000	65 276	175	−111
(PEI/HNT/PEI/$CuPc^{SO3-}$)$_5$	450 990	91 310	180	−126
(PEI/HNT/PEI/$CuPc^{SO3-}$)$_{10}$	475 980	115 381	180	−190

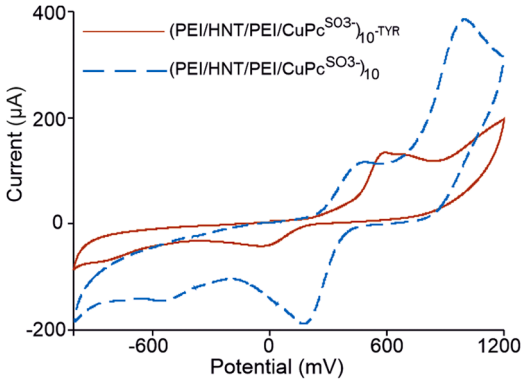

Fig. 8. Voltammetric responses of the (PEI/HNT/PEI/$CuPc^{SO3-}$)$_{10}$-Tyr-sensor compared to the non-enzymatic sensor in 10^{-3} mol·L^{-1} catechol in KCl (0.1 mol·L^{-1}).

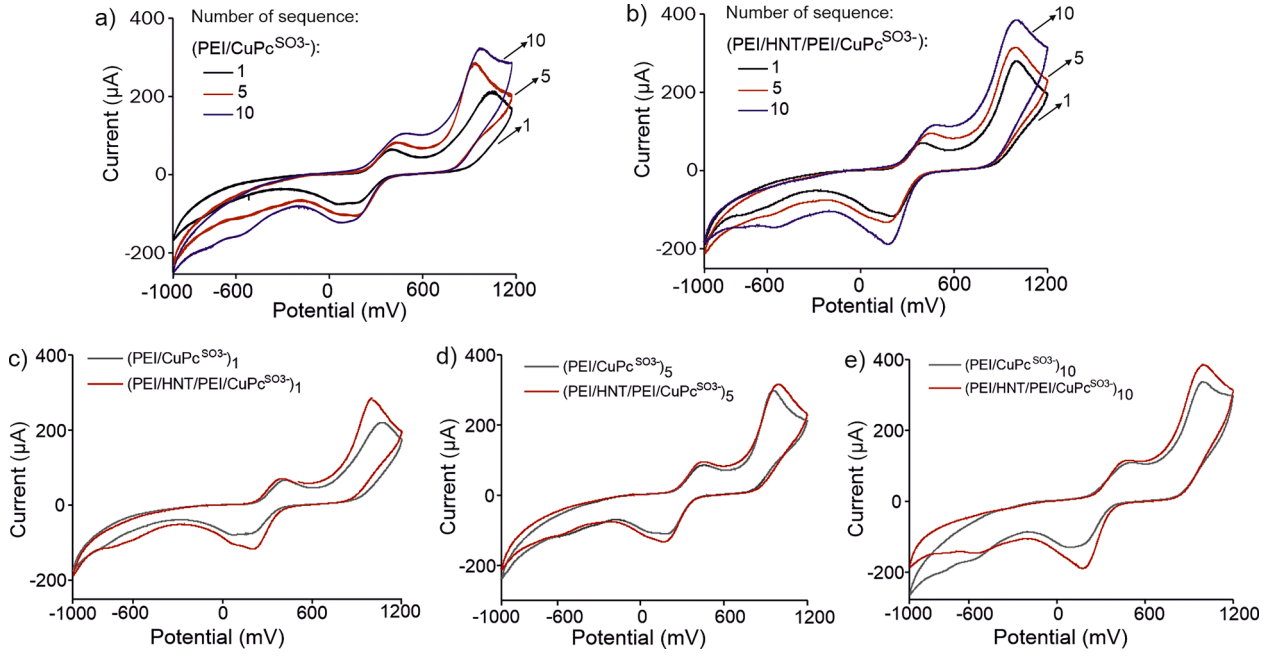

Fig. 7. Voltammetric responses in 10^{-3} mol·L^{-1} catechol in KCl (0.1 mol·L^{-1}) for (a) the (PEI/$CuPc^{SO3-}$) sensor, (b) the (PEI/HNT/PEI/$CuPc^{SO3-}$) sensor, and (c-e) comparison of voltammograms for each LbL sensor and for different number of sequences.

3.4. Limits of detection and scan rate study

The limits of detection (LD) were evaluated by analysing the response of the LbL sensors (elaborated with 10 sequences) towards catechol at different concentrations ranging from 10 to 138 μmol·L^{-1}. The results are illustrated in Fig. 9 for the (PEI/CuPc^{SO3-})$_{10}$ and the (PEI/HNT/PEI/CuPc^{SO3-})$_{10}$ LbL sensors. The study was carried out evaluating the anodic peak at 420–425 mV observed for (PEI/CuPc^{SO3-})$_{10}$ and (PEI/HNT/PEI/CuPc^{SO3-})$_{10}$ sensors. In both cases, a linear relationship was observed between the intensities and the concentration of catechol, confirming the availability of these LbL sensors to determine this compound. The limits of detection, using the "3·SD/m" criterion, were 1.23·10^{-6} mol·L^{-1} for the (PEI/CuPc^{SO3-})$_{10}$ sensor and slightly better for the (PEI/HNT/PEI/CuPc^{SO3-})$_{10}$, reaching a LD of 9.87·10^{-7} mol·L^{-1}. In addition, as the coefficient of regression was quite higher for the (PEI/HNT/PEI/CuPc^{SO3-})$_{10}$ sensor (r^2 = 0.973) in comparison to the (PEI/CuPc^{SO3-}) sensor (r^2 = 0.926), this result confirmed the more reliability of the (PEI/HNT/PEI/CuPc^{SO3-})$_{10}$ sensors.

The improved performance can be attributed to synergistic interactions between the HNT and the phthalocyanine in terms of a better adhesion of the latter in the structure of the films. This improvement was also confirmed by carrying out a scan rate dependence study in order to observe the influence of the HNT in the electron transfer behaviour of the sensors. For this purpose, voltammograms in catechol 10^{-3} mol·L^{-1} were collected at different scan rates ranging from 10 to 2000 mV·s^{-1}. The responses are illustrated in Fig. 10.

The cathodic and anodic peak potentials shifted to more negative and positive potentials, respectively, with increasing the scan rate. The anodic peak currents (I_a) varied linearly with the square root of the scan rate ($v^{1/2}$). These results indicate that the redox processes of catechol on the (PEI/CuPc^{SO3-})$_{10}$ and (PEI/HNT/PEI/CuPc^{SO3-})$_{10}$ sensors are controlled by diffusion [43,44] according to the Randles-Sevick Eq. (1):

$$I_a = 2.65 \cdot 10^5 \cdot n^{3/2} \cdot D^{1/2} \cdot v^{1/2} \cdot A \cdot C \quad (1)$$

Where I_a is the anodic peak current, n is the electron number, D is the diffusion coefficient of catechol, v is the scan rate, A is the electroactive area of the electrode (cm^2) and C is the concentration of catechol (mol·cm^{-3}). According to the slope values, the higher value for the (PEI/HNT/PEI/CuPc^{SO3-})$_{10}$ sensor indicated that the oxidation of catechol occurred more rapidly in that sensor due to the electroactive area of the electrode is higher according to Eq. (1), confirming the improvement of the electron transfer rates.

The specificity of the (PEI/HNT/PEI/CuPc^{SO3-})$_{10}$ sensors was improved incorporating tyrosinase in the structure. In Fig. 11 can be observed that when representing the catechol concentration vs. the current of the anodic peak obtained from the enzymatic LbL sensor, a linear relationship was obtained in the concentration range with a regression coefficient of 0.9967, higher than for the non-enzymatic sensor. The limit of detection obtained with (PEI/HNT/PEI/CuPc^{SO3-})$_{10}$-Tyr-sensor was 9.38·10^{-7} mol·L^{-1}, which was similar to that obtained with the non-enzymatic sensor. However, the higher coefficient of regression confirmed the higher reliability of the (PEI/HNT/PEI/CuPc^{SO3-})$_{10}$-Tyr-sensor compared to the non-enzymatic sensor.

The electrochemical performance of the LbL tyrosinase biosensor was compared with others reported in the literature (Table 2). It can be seen that the linear range, detection limit and sensitivity were comparable, and/or even superior, with the results obtained in other research group's work. Moreover, the simple procedure for the construction of the reported biosensor means a significant advantage in comparison with others.

PEDOT/PSS: poly (3,4-ethylenedioxythiophene)/polystyrene sulfonate; AuNPs: gold nanoparticles; IL: ionic liquid; MWCNT: multi-walled carbon nanotube; DHP: dihexadecylphosphate; GCE: glassy carbon electrode; AgNWs: silver nanowires; PPy: polypyrrole; Pt: platinum electrode; MNP: magnetic nanoparticles; SPE: screen-printed electrode; SPCE: screen-printed carbon electrode; GA: glutaraldehyde; pTH: poly (thionine); PAPCP: poly(N-3-aminopropyl pyrrole-co-pyrrole); ITO: indium-tin-oxide; AEP: acetone-extracted propolis; Au: gold electrode.

3.5. Repeatability and reproducibility

The reproducibility and repeatability of the sensors was examined by cycling the electrodes in catechol 10^{-3} mol·L^{-1} using three electrodes prepared at different days and using 10 sequences in the LbL film construction. The reproducibility of the LbL method was confirmed since coefficients of variation lower than 4 % were found in both, the cathodic and anodic peaks. Regarding the repeatability, the results of 5 consecutive cycles showed a coefficient of variation lower than 2 % for the non-enzymatic sensors and lower than 5 % for the (PEI/HNT/PEI/CuPc^{SO3-})$_{10}$-Tyr-sensor.

4. Conclusions

This work provides a study of a LbL sensor based on HNTs in order to enhance the electrochemical performance of the sensors. The UV–Vis characterization corroborated the adhesion of CuPc^{SO3-} on the LbL films, with a higher level of organization in the LbL structure when using HNT in the growth of the films. Moreover, the electrostatic interaction between the materials used in the LbL films was confirmed by using FTIR characterization. In addition, important advantages have been evidenced due to the incorporation of HNT in the enzymatic biosensor

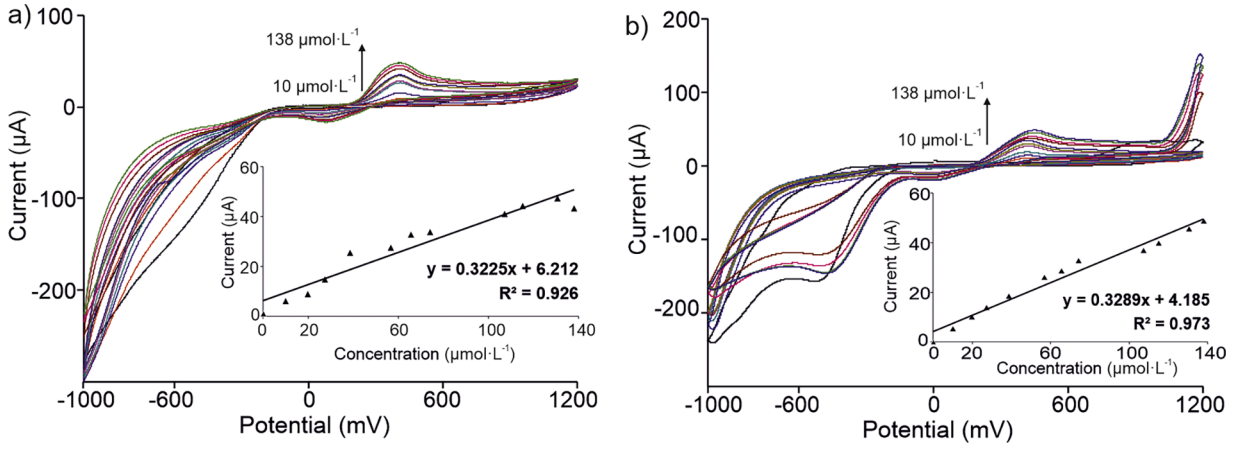

Fig. 9. Voltammograms and linear relationship between intensity and concentration of (a) (PEI/CuPc^{SO3-})$_{10}$ and (b) (PEI/HNT/PEI/CuPc^{SO3-})$_{10}$ sensors immersed in increasing concentrations of catechol ranging from 10 to 138 μmol·L^{-1}.

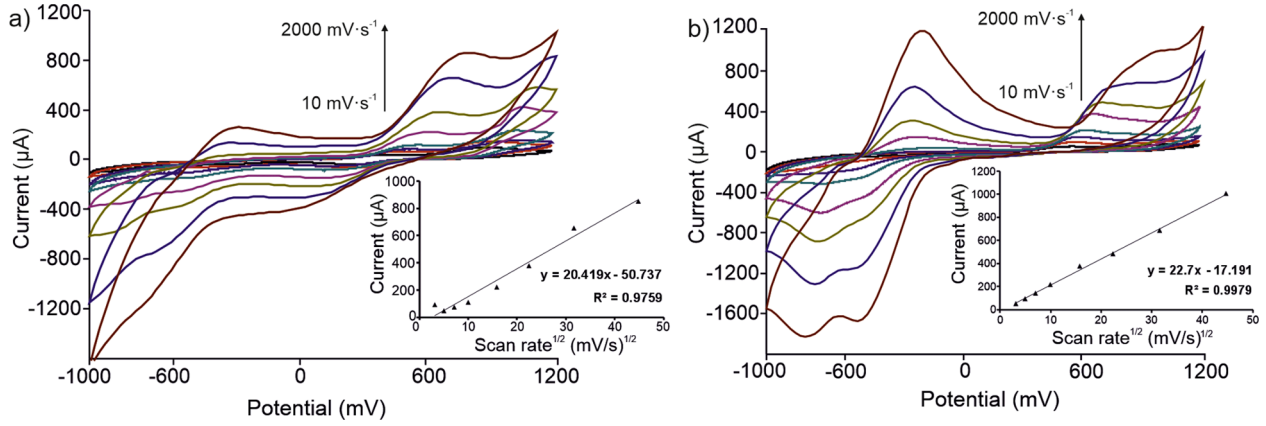

Fig. 10. Voltammograms and linear relationship between I_a and $v^{1/2}$ of (a) (PEI/CuPc^{SO3-})$_{10}$ and (b) (PEI/HNT/PEI/CuPc^{SO3-})$_{10}$ sensors (immersed in 10^{-3} mol·L^{-1} catechol in KCl (0.1 mol·L^{-1}) at scan rates ranging from 10 to 2000 mV·s^{-1}).

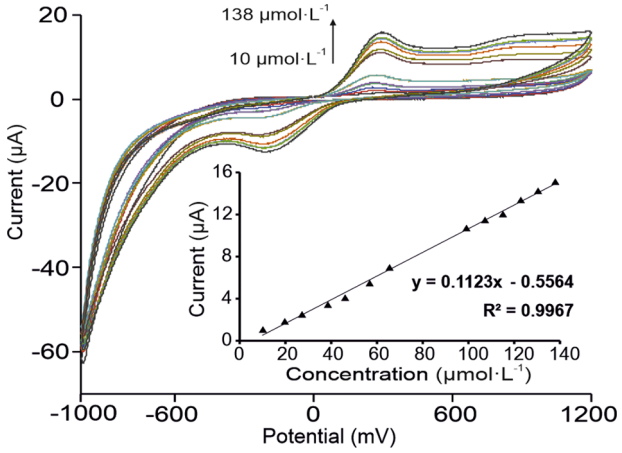

Fig. 11. CVs and linear relationship between intensity and concentration of the (PEI/HNT/PEI/CuPc^{SO3-})$_{10}$-Tyr-sensor immersed in increasing concentrations of catechol ranging from 10 to 138 μmol·L^{-1}.

based on tyrosinase. The results showed that the presence of HNT in the LbL sensor gives voltammetric responses with redox peaks with higher intensities. Moreover, the electroactive area of the HNT based sensor was higher leading to a more rapidly oxidation of catechol. In addition, the limits of detection were improved when using HNT in the LbL structure as well as the reliability of the results was higher. The use of tyrosinase to construct an enzymatic sensor based on HNT and LbL exhibited redox peaks with lower intensities, but more reversible, and limits of detection similar to that obtained with the non-enzymatic sensors. However, the high coefficient of regression obtained confirmed a higher reliability when using tyrosinase. In addition, the linear range, detection limit and sensitivity of the tyrosinase biosensor were comparable, and/or even superior, with other catechol biosensors based on tyrosinase. Finally, the LbL sensor and biosensor showed excellent reproducibility and repeatability that could be attributed to the reliability of LbL procedure.

Table 2
Comparison with other catechol biosensors based on tyrosinase.

Tyrosinase-based biosensors	Linear range (μmol·L^{-1})	Detection limit (μmol·L^{-1})	Sensitivity (mA·mol^{-1}·L)	Reference
PEDOT/PSS/AuNP-Tyr	4–60	0.39	–	[45]
PEDOT/PSS/AuNP-Tyr	90–150	2.80	–	[45]
TYR-IL-MWCNT-DHP/GCE	4.9–1100	0.58	–	[46]
AgNWs-Tyr	25–172	2.70	197.9	[47]
Tyr-AuNPs-DHP/GCE	2.5–95	0.17	115	[48]
Tyr-PO$_4$–PPy/Pt	10–120	0.84	47	[49]
Tyr-MWCNT-MNP/SPE	10–80	7.61	–	[50]
Tyr-AuNPs-SPCE	2.5–20	1.2	55	[51]
TYR/GA/pTN/GCE	1–300	6	–	[52]
Tyr-PAPCP/ITO	1.6–119	1.2	3.46	[53]
Tyr/MWCNT/AuNPs/AEP/Au	1–500	0.80	150	[54]
(PEI/HNT/PEI/CuPc^{SO3-})$_{10}$-Tyr	10–138	0.94	112.3	This work

CRediT authorship contribution statement

C. Garcia-Hernandez: Conceptualization, Data curation, Formal analysis, Investigation, Methodology, Supervision, Validation, Writing – original draft, Writing – review & editing. **C. Garcia-Cabezon:** Conceptualization, Writing – original draft, Funding acquisition, Project administration, Writing – review & editing, Supervision. **M.L. Rodriguez-Mendez:** Funding acquisition, Conceptualization, Project administration, Writing – original draft, Supervision, Writing – review & editing. **F. Martin-Pedrosa:** Data curation, Conceptualization, Supervision, Funding acquisition, Project administration, Software.

Declaration of Competing Interest

The authors declare that they have no known competing financial interests or personal relationships that could have appeared to influence the work reported in this paper.

Data availability

Data will be made available on request.

Acknowledgments

We appreciate the financial support of MINECO-FEDER Plan Nacional (PID2021-122365OB-100). Junta de Castilla y Leon- FEDER

VA202P20. BIOECOUVA-CLU-2019-04 and «Infraestructuras Red de Castilla y León (INFRARED)» UVA01.

References

[1] A. Legin, S. Makarychev-Mikhailov, O. Goryacheva, D. Kirsanov, Y. Vlasov, Cross-sensitive chemical sensors based on tetraphenylporphyrin and phthalocyanine, Anal. Chim. Acta 457 (2002) 297–303, https://doi.org/10.1016/S0003-2670(02)00052-1.

[2] M.L. Rodriguez-Mendez, M. Gay, J.A. de Saja, New insights into sensors based on radical bisphthalocyanines, J. Porphyr. Phthal. 13 (2009) 1159–1167, https://doi.org/10.1142/S1088424609001509.

[3] J.H. Zagal, S. Griveau, J.F. Silva, T. Nyokong, F. Bedioui, Metallophthalocyanine-based molecular materials as catalysts for electrochemical reactions, Coord. Chem. Rev. 254 (2010) 2755–2791, https://doi.org/10.1016/j.ccr.2010.05.001.

[4] M.L. Rodriguez-Mendez, C. Medina-Plaza, J.A. de Saja, C. Apetrei, R. Muñoz, Sensor arrays based on phthalocyanines: new developments on nanostructured and biomimetic electrochemical sensors, in: L. Lvova, D. Kirsanov, C. Di Natale, A. Legin (Eds.), Multisensor Systems For Chemical analysis: Materials and Sensors, Pan Stanford Publishing, Singapore, 2012, pp. 70–109.

[5] S. Fabiano, S. Braun, X. Liu, E. Weverberghs, P. Gerbaux, M. Fahlman, M. Berggren, X. Crispin, Poly(ethylene imine) impurities induce n-doping reaction in organic (Semi)conductors, Adv. Mater. (2014), https://doi.org/10.1002/adma.201401986.

[6] J.C. Scott, Metal–organic interface and charge injection in organic electronic devices, J. Vac. Sci. Technol. A 21 (2003) 521, https://doi.org/10.1116/1.1559919.

[7] Y.L. Shen, A.R. Hosseini, M.H. Wong, G.G. Malliaras, How to make ohmic contacts to organic semiconductors, ChemPhysChem 5 (2004) 16–25, https://doi.org/10.1002/cphc.200300942.

[8] T. Matsushima, Y. Kinoshita, H. Murata, Formation of Ohmic hole injection by inserting an ultrathin layer of molybdenum trioxide between indium tin oxide and organic hole-transporting layers, Appl. Phys. Lett. 91 (2007), 253504, https://doi.org/10.1063/1.2825275.

[9] Y.H. Zhou, C. Fuentes-Hernandez, J. Shim, J. Meyer, A.J. Giordano, H. Li, P. Winget, T. Papadopoulos, H. Cheun, J. Kim, M. Fenoll, A. Dindar, W. Haske, E. Najafabadi, T.M. Khan, H. Sojoudi, S. Barlow, S. Graham, J.L. Bredas, S. R. Marder, A. Kahn, B. Kippelen, A universal method to produce low-work function electrodes for organic electronics, Science 336 (2012) 327–332, https://doi.org/10.1126/science.1218829.

[10] F. Bergaya, G. Lagaly, Chapter 1—General introduction: clays, clay minerals, and clay science, in: F. Bergaya, G.B.T.-D. Lagaly (Eds.), Handbook of Clay Science, Elsevier, Amsterdam, The Netherlands, 2013, pp. 1–19. ISBN 1572-4352.

[11] K. Song, Micro- and nano-fillers used in the rubber industry, Prog. Rubber Nanocompos. 2017 (2017) 41–80, https://doi.org/10.1016/b978-0-08-100409-8.00002-4.

[12] E. Pavón, R. Martín-Rodríguez, A.C. Perdigón, M.D. Alba, New trends in nanoclay-modified sensors, Inorganics 9 (2021) 43, https://doi.org/10.3390/inorganics9060043.

[13] E.S. Goda, M.A. Gab-Allah, B.S. Singu, K.R. Yoon, Halloysite nanotubes based electrochemical sensors: a review, Microchem. J. 147 (2019) 1083–1096, https://doi.org/10.1016/j.microc.2019.04.011.

[14] N. Khatri, S. Tyagi, D. Rawtani, Removal of basic dyes auramine yellow and auramine O by halloysite nanotubes, Int. J. Environ. Waste Manag. 17 (2016) 44–59, https://doi.org/10.1504/IJEWM.2016.076427.

[15] M. Tharmavaram, G. Pandey, D. Rawtani, Surface modified halloysite nanotubes: a flexible interface for biological, environmental and catalytic applications, Adv. Colloid Interface Sci. 261 (2018) 82–101, https://doi.org/10.1016/j.cis.2018.09.001.

[16] D. Rawtani, Y.K. Agrawal, Halloysite as support matrices: a review, Emerg. Mater. Res. 1 (2012) 212–220, https://doi.org/10.1680/emr.12.00005.

[17] D. Rawtani, Y.K. Agrawal, A study of the behavior of HNT with DNA intercalator acridine orange, BioNanoSci 3 (2013) 52–57, https://doi.org/10.1007/s12668-012-0066-1.

[18] Z. Yang, X. Zheng, J. Zheng, Non-enzymatic sensor based on a glassy carbon electrode modified with ag nanoparticles/polyaniline/halloysite nanotube nanocomposites for hydrogen peroxide sensing, RSC Adv. 6 (2016) 58329–58335, https://doi.org/10.1039/C6RA06366G.

[19] S. Zhang, Q. Sheng, J. Zheng, Synthesis of Ag-HNTs-MnO2 nanocomposites and their application for nonenzymatic hydrogen peroxide electrochemical sensing, RSC Adv. 5 (2015) 26878–26885, https://doi.org/10.1039/C5RA01390A.

[20] H. Cao, X. Sun, Y. Zhang, N. Jia, Electrochemical sensing based on gold nanoparticle-decorated halloysite nanotube composites, Anal. Biochem. 430 (2012) 111–115, https://doi.org/10.1016/j.ab.2012.08.014.

[21] Q. Sheng, D. Zhang, Q. Wu, J. Zheng, H. Tang, Electrodeposition of prussian blue nanoparticles on polyaniline coated halloysite nanotubes for nonenzymatic hydrogen peroxide sensing, Anal. Methods 7 (2015) 6896–6903, https://doi.org/10.1039/C5AY01329A.

[22] R. Cheng, Q. Zou, X. Zhang, C. Xiao, L. Sun, J. Chen, Template synthesis of nitrogen-doped short tubular carbons with big inner diameter and their application in electrochemical sensing, Bull. Kor. Chem. Soc. 35 (2014) 2423–2430, https://doi.org/10.5012/bkcs.2014.35.8.2423.

[23] M. Ghanei-Motlagh, M. Taher, A novel electrochemical sensor based on silver/halloysite nanotube/molybdenum disulfide nanocomposite for efficient nitrite sensing, Biosens. Bioelectron. 109 (2018) 279–285, https://doi.org/10.1016/j.bios.2018.02.057.

[24] S. Zhang, Q. Sheng, J. Zheng, Synthesis of Au nanoparticles dispersed on halloysite nanotubes-reduced graphene oxide nanosheets and their application for nitrites electrochemical sensing, New J. Chem. 40 (2016) 9672–9678, https://doi.org/10.1039/C6NJ02103D.

[25] W. Wang, K. Jiang, X. Zhang, J. Chen, A high-performance bioanode based on a nitrogen-doped short tubular carbon loaded au nanoparticle co-immobilized mediator and glucose oxidase for glucose/O2 biofuel cells, RSC Adv. 6 (2016) 29142–29148, https://doi.org/10.1039/c6ra02817a.

[26] Q. Wu, Q. Sheng, J. Zheng, Nonenzymatic sensing of glucose using a glassy carbon electrode modified with halloysite nanotubes heavily loaded with palladium nanoparticles, J. Electroanal. Chem. 762 (2016) 51–58, https://doi.org/10.1016/j.jelechem.2015.12.030.

[27] L. Shao, Xi. Wang, B. Yang, Q. Wang, Q. Tian, Z. Ji, J. Zhang, A highly sensitive ascorbic acid sensor based on hierarchical polyaniline coated Halloysite nanotubes prepared by electrophoretic deposition, Electrochim. Acta 255 (2017) 286–297, https://doi.org/10.1016/j.electacta.2017.09.178.

[28] B. Xing, X. Yin, Novel poly-dopamine adhesive for a Halloysite nanotube-Ru (bpy)3 2+ electrochemiluminescent sensor, PLoS ONE 4 (7) (2009) e6451, https://doi.org/10.1371/journal.pone.0006451.

[29] X. Zhang, Q. Sheng, J. Zheng, Preparation of tubular HNTs@PDA–Au nanocomposites and its electrocatalysis of hydrazine, Nano 13 (2018), 1850019, https://doi.org/10.1142/S1793292018500194.

[30] M. Fayazia, M. Taher, D. Afzali, A. Mostafavi, Fe3O4 and MnO2 assembled on halloysite nanotubes: a highly efficient solid-phase extractant for electrochemical detection of mercury(II) ions, Sens. Actuators B Chem. 228 (2016) 1–9, https://doi.org/10.1016/j.snb.2015.12.107.

[31] S. Kumar-Krishnan, A. Hernandez-Rangel, U. Pal, O. Ceballos-Sanchez, F.J. Flores-Ruiz, E. Prokhorov, O. Arias de Fuentes, R. Esparza, M. Meyyappan, Surface functionalized halloysite nanotubes decorated with silver nanoparticles for enzyme immobilization and biosensing, J. Mater. Chem. B 4 (2016) 2553–2560, https://doi.org/10.1039/C6TB00051G.

[32] C. Chao, J. Liu, J. Wang, Y. Zhang, B. Zhang, Y. Zhang, X. Xiang, R. Chen, Surface modification of halloysite nanotubes with dopamine for enzyme immobilization, ACS Appl. Mater. Interfaces 5 (2013) 10559–10564, https://doi.org/10.1021/am4022973.

[33] D. Brondani, C. Scheeren, J. Dupont, I. Vieira, Halloysite clay nanotubes and platinum nanoparticles dispersed in ionic liquid applied in the development of a catecholamine biosensor, Analyst 21 (2012) 3732–3739, https://doi.org/10.1039/c2an35313j.

[34] C. García-Hernández, C. Medina-Plaza, C. García-Cabezón, F. Martín-Pedrosa, I. del Valle, J.A. de Saja, M.L. Rodríguez-Méndez, An electrochemical quartz crystal microbalance multisensor system based on phthalocyanine nanostructured films: discrimination of musts, Sensors 15 (2015) 29233–29249, https://doi.org/10.3390/s151129233.

[35] C. Salvo-Comino, A. González-Gil, J. Rodriguez-Valentin, C. Garcia-Hernandez, F. Martin-Pedrosa, C. Garcia-Cabezon, M.L. Rodriguez-Mendez, Biosensors platform based on Chitosan/AuNPs/Phthalocyanine composite films for the electrochemical detection of catechol. the role of the surface structure, Sensors 10 (7) (2020) 2152, https://doi.org/10.3390/s20072152, 20.

[36] C. Salvo-Comino, C. Garcia-Hernandez, C. Garcia-Cabezon, M.L. Rodriguez-Mendez, Promoting laccase sensing activity for catechol detection using LBL assemblies of chitosan/ionic liquid/phthalocyanine as immobilization surfaces, Bioelectrochemistry 132 (2020), 107407, https://doi.org/10.1016/j.bioelechem.2019.107407.

[37] N.C. de Lucena, C.M. Miyazaki, F.M. Shimizu, C.J.L. Constantino, M. Ferreira, Layer-by-layer composite film of nickel phthalocyanine and montmorillonite clay for synergistic effect on electrochemical detection of dopamine, Appl. Surf. Sci. 436 (2018) 957–966, https://doi.org/10.1016/j.apsusc.2017.12.117.

[38] W. Li, J. Wu, S.S. Lee, J.D. Fortner, Surface tunable magnetic nano-sorbents for carbon dioxide sorption and separation, Chem. Eng. J. 313 (2017) 1160–1167, https://doi.org/10.1016/j.cej.2016.11.013.

[39] S.S. Patel, D.B. Patel, A.K. Poddar, J.B. Patel, D.N. Rana, K.P. Patel, S.P. Thakar, H. D. Patel, Copper phthalocyanine tetrasulfonic acid (CuPcS) as an efficient recyclable catalyst for aromatic nitration using sodium nitrate, J. Mol. Struct. 1280 (2023), 135039, https://doi.org/10.1016/j.molstruc.2023.135039.

[40] M. Norman, J. Zdarta, P. Bartczak, A. Piasecki, I. Petrenko, H. Ehrlich, T. Jesionowski, Marine sponge skeleton photosensitized by copper phthalocyanine: a catalyst for Rhodamine B degradation, Open Chem. 14 (2016) 243–254, https://doi.org/10.1515/chem-2016-0025.

[41] P.R. Chang, Y. Xie, D. Wu, X. Ma, Amylose wrapped halloysite nanotubes, Carbohydr. Polym. 84 (2011) 1426–1429, https://doi.org/10.1016/j.carbpol.2011.01.038.

[42] V. Zucolotto, M. Ferreira, M.R. Cordeiro, C.J.L. Constantino, D.T. Balogh, A. R. Zanatta, W.C. Moreira, O.N. Oliveira, Unusual interactions binding irontetrasulfonated phthalocyanine and poly(allylamine hydrochloride) inlayer-by-layer films, J. Phys. Chem. B 107 (2003) 3733–3737, https://doi.org/10.1021/jp027573d.

[43] A.I. Ruiz-Carmuega, C. Garcia-Hernandez, J. Ortiz, C. Garcia-Cabezon, F. Martin-Pedrosa, A. Sastre-Santos, M.A. Rodríguez-Perez, M.L. Rodriguez-Mendez, Electrochemical sensors modified with combinations of sulfur containing phthalocyanines and capped gold nanoparticles: a study of the influence of the nature of the interaction between sensing materials, Nanomaterials 9 (2019) 1506, https://doi.org/10.3390/nano9111506.

[44] C. Medina-Plaza, C. García-Cabezón, C. García-Hernández, C. Bramorski, Y. Blanco-Val, F. Martín-Pedrosa, T. Kawai, J.A. de Saja, M.L. Rodríguez-Méndez, Analysis of organic acids and phenols of interest in the wine industry using Langmuir–Blodgett films based on functionalized nanoparticles, Anal. Chim. Acta 853 (2015) 572–578, https://doi.org/10.1016/j.aca.2014.10.046.

[45] C. García-Hernández, C. García-Cabezón, F. Martín-Pedrosa, J.A. De Saja, M. L. Rodríguez-Méndez, Layered composites of PEDOT/PSS/nanoparticles and PEDOT/PSS/phthalocyanines as electron mediators for sensors and biosensors, Beilstein J. Nanotechnol. 7 (2016) 1948–1959, https://doi.org/10.3762/bjnano.7.186.

[46] F.C. Vincentini, B.C. Janegitz, C.M.A. Brett, O. Fatibello-Filho, Tyrosinase biosensor based on a glassy carbon electrode modified with multi-walled carbon nanotubes and 1-butyl-3-methylimidazolium chloride within a dihexadecylphosphate film, Sens. Actuators, B 188 (2013) 1101, https://doi.org/10.1016/j.snb.2013.07.109.

[47] C. Salvo-Comino, F. Martin-Pedrosa, C. Garcia-Cabezon, M.L. Rodriguez-Mendez, Nanowires as electron transfer mediators in electrochemical catechol biosensors, Sensors 21 (2021) 899, https://doi.org/10.3390/s21030899.

[48] F.C. Vicentini, L.L.C. Garcia, L.C.S. Figueiredo-Filho, B.C. Janegitz, O. Fatibello-Filho, A biosensor based on gold nanoparticles, dihexadecylphosphate, andtyrosinase for the determination of catechol in natural water, Enzyme Microb. Technol. 84 (2016) 17–23, https://doi.org/10.1016/j.enzmictec.2015.12.004.

[49] C. Apetrei, M.L. Rodriguez-Mendez, J.A. De Saja, Amperometric tyrosinasebased biosensor using an electropolymerized phosphate-doped polypyrrolefilm as an immobilization support. Application for detection of phenoliccompounds, Electrochim. Acta 56 (2011) 8919–8925, https://doi.org/10.1016/j.electacta.2011.07.127.

[50] B. Perez-Lopez, A. Merkoci, Magnetic nanoparticles modified with carbonnanotubes for electrocatalytic magnetoswitchable biosensing applications, Adv. Funct. Mater. 21 (2011) 255–260, https://doi.org/10.1002/adfm.201001306.

[51] M. Cerrato-Alvarez, E. Bernalte, M.J. Bernalte-García, E. Pinilla-Gil, Fast and direct amperometric analysis of polyphenols in beers using tyrosinase-modified screen-printed gold nanoparticles biosensors, Talanta 193 (2019) 93–99, https://doi.org/10.1016/j.talanta.2018.09.093.

[52] ZhenYong Lu, Yue Wang, Zhiqiang Zhang, Yang Shen, Mengfan Li, Tyrosinase modified poly(thionine) electrodeposited glassy carbon electrode for amperometric determination of catechol, Electrochemistry 85 (2017) 17–22, https://doi.org/10.5796/electrochemistry.85.17.

[53] W.T. Rajesh, K. Kaneto, Amperometric phenol biosensor based oncovalent immobilization of tyrosinase onto an electrochemically preparednovel copolymer poly(N-3-aminopropyl pyrrole-co-pyrrole) film, Sens. Actuators B 102 (2004) 271–277, https://doi.org/10.1016/j.snb.2004.04.028.

[54] F. Kheiri, R.E. Sabzi, E. Jannatdoust, H. Sedghi, Acetone extracted propolis as anovel membrane and its application in phenol biosensors: the case of catechol, J. Solid State Electrochem. 15 (2011) 2593–2599, https://doi.org/10.1007/s10008-010-1250-2.